Inner Current Loop Analysis and Design Based on Resonant Regulators for Isolated Microgrids

Federico, de Bosio; de Sousa Ribeiro, Luiz Antonio ; Soares Lima, Marcel; Freijedo Fernandez, Francisco Daniel; Guerrero, Josep M.; Pastorelli, Michelle

Published in:
13th Brazilian Power Electronics Conference

DOI (link to publication from Publisher):
10.1109/COBEP.2015.7420244

Publication date:
2015

Document Version
Early version, also known as pre-print

INNER CURRENT LOOP ANALYSIS AND DESIGN BASED ON RESONANT REGULATORS FOR ISOLATED MICROGRIDS

Federico de Bosio[1], Luiz A. de S. Ribeiro[2], M. S. Lima[2], Francisco Freijedo[3], J. M. Guerrero[3], M. Pastorelli[1]
[1]Energy Department/Politecnico di Torino, Torino, Italy
[2]Institute of Electrical Energy/Federal University of Maranhão, São Luís-MA, Brazil
[3]Department of Energy Technology/Aalborg University, Aalborg, Denmark
e-mail: federico.debosio@polito.it; l.a.desouzaribeiro@ieee.org; michele.pastorelli@polito.it; fran@et.aau.dk; joz@et.aau.dk

***Abstract*— Inner current and voltage loops are fundamental in achieving good performance of microgrids based on power electronics voltage source inverters. The analysis and design of these loops are essential for the adequate operation of these systems. This paper investigates the effect of state feedback coupling in the design of proportional resonant controllers for these inner loops in voltage source inverters operating in islanded microgrids. It is also shown that the state feedback coupling has an important effect in the performance of the control loops by increasing the steady-state error. A comparison between different types of proportional+resonant controllers is done. Experimental results verify the theoretical assumptions done.**

Keywords—voltage and current regulation; proportional+resonant (PR), complex vector PR

I. INTRODUCTION

Voltage and current regulation play an important role in modern applications of power electronics, such as variable speed drives, active power filters, and microgrids [1],[2],[3]. The general power processor unit used in these applications is the Voltage Source Inverter (VSI) operating in current or voltage control depending on the application. The inner loops are responsible for controlling torque in AC machines, harmonic compensation in active power filters and microgrids, and voltage regulation in isolated microgrids. Hence, accurate control of current, voltage or both is required for the VSI to succeed in implementing the desired feature of each application. It is expected from any current or voltage regulator to [3],[4]: *i*) achieve zero steady-state error; *ii*) accurately track the commanded reference during transients; *iii*) bandwidth as higher as possible; and *iv*) decrease or minimize low order harmonics.

Linear regulators suit very well for analysis with classical control theory. Among linear controllers the synchronous reference frame proportional integral (PI) [4], and proportional resonant (PR) [5] are the most common regulators used in these applications. Due to the importance of these regulators, there has been substantial research activity in the subject throughout the years [6-9].

PR controllers avoid the rotations used in synchronous PI regulators and can be used in single-phase systems. The PR controller [5] is derived from two synchronous frame PI regulators [4], but it is implemented in the stationary reference frame. In some applications, non-ideal PR is used to avoid implementation problems in low cost processors. Another implementation, called complex vector PR was initially applied in sensorless AC drives [10]. It is derived from two complex vector PIs [11] and is implemented in the stationary reference frame.

This paper addresses different current control implementations based on resonant controllers for VSI connected in isolated microgrids. Even though extensive research has been done in systems with a strong electromotive force (emf), the isolated microgrid structure has not been previously discussed in depth. In such cases, the coupling between the capacitor voltage and inductor current plays an important role in the performance of PR regulators. The aim of this paper is to analyze the performance of PR regulators, the effect of voltage coupling in the performance of these regulators, and the fundamental differences between the PR controllers.

II. SYSTEM DESCRIPTION

The control of parallel-connected VSIs in isolated microgrids is based on droop control strategy that provides the voltage and frequency references for the inner loops [3]. In isolated microgrids the VSI operates in voltage mode where the capacitor voltage and inductor currents are the controlled states. The block diagram including three-phase three-legs inverter with its respective inner loops is presented in Fig. 1. The goal of the inner current loop is to track the references provided by the secondary loops. Whenever the current regulators are unable to perform properly this goal the system performance degrades. Therefore, analyzing the behavior of the inner current loops is important to understand and propose solutions to improve their performance.

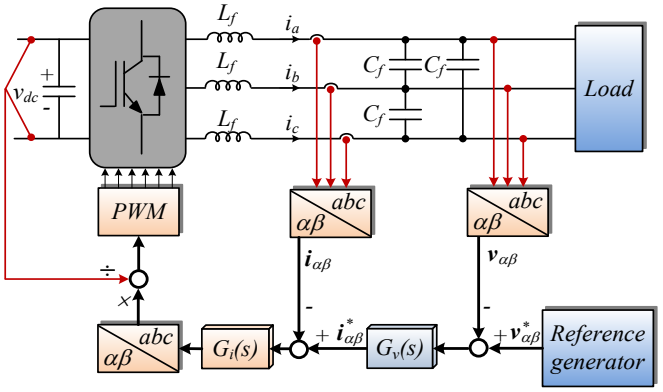

Fig. 1. Block diagram of a three phase VSI with voltage and current loops

The simplified control block diagram of closed-loop system is shown in Fig. 2, where $\boldsymbol{v}^*_{\alpha\beta}$ and $\boldsymbol{i}^*_{\alpha\beta}$ are the reference voltage and current vectors, $\boldsymbol{i}_{o\alpha\beta}$ is the output current vector, L_f is the filter inductor, R_f is the equivalent series resistance of the inductor, and C_f is the filter capacitor. $G_i(s)$ and $G_v(s)$ represent the current and voltage regulators transfer functions, and $G_{pwm}(s) = [1 - (T_d/2)s]/[1 + (T_d/2)s]$ is the transfer function related to computation and PWM delays. $G_{dec}(s)$ is the transfer function related to the decoupling between the capacitor voltage and inductor current. It must be designed to compensate for the delay introduced by the control and PWM, otherwise the decoupling will not be ideal.

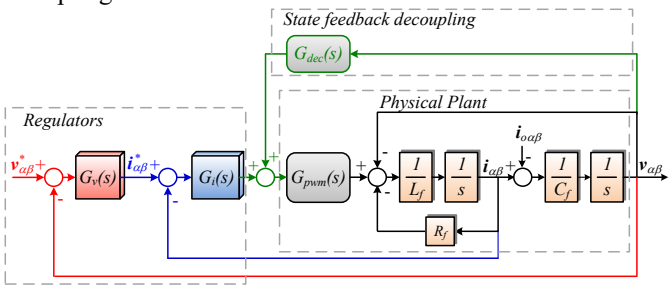

Fig. 2. Simplified block diagram of the closed-loop system

The first loop to be considered is the current one. If the cross-coupling decoupling is not performed, the block diagram used for tuning the current loop is presented in Fig. 3. The parameters of the system used to perform the analysis are presented in TABLE I. The system is implemented using a VSI operating with regular sampling symmetrical PWM. As a result the delay introduced by the PWM update and control is $T_d = 1.5T_s = 150\ \mu s$.

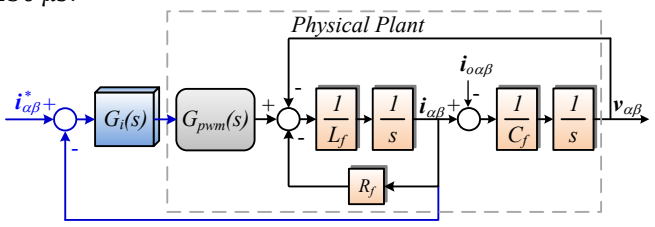

Fig. 3. Block diagram for the design of the current regulator

TABLE I. SYSTEM PARAMETERS

Parameter	Symbol	Value
Line to line voltage	v_{gll}	380 V
Fundamental frequency	f_g	50 Hz
Rated power	P_{nom}	2.2 kW
Rated current	i_{snom}	3.33 A
Switching frequency	f_{sw}	10 kHz
Sampling period	T_s	100 µs
Filter inductance	L_f	1.8 mH
Filter capacitance	C_f	27 µF
Inductor ESR	R_f	0.1 Ω
Rated load resistance	R_l	68 Ω

As a benchmark for comparison and due to its simplicity, the proportional controller is used. In addition, a bandwidth for the inner current loop equal to 1 kHz is considered. The general approach to design this loop is to neglect the capacitor cross-coupling that can be treated as a disturbance. This is the basic assumption in AC drives and grid connected application, as the emf is strong, and acts as disturbance to the current regulator. However, due to the cross-coupling between the capacitor voltage and inductor current, the assumption that the voltage can be treated as a disturbance does not hold true anymore. Therefore, the root locus of the system is presented in Fig. 4. This root locus shows that due to the right half plane zero (non-minimal phase zero) introduced by the delay the system can become unstable for certain gain values. The open loop dominant poles (see Fig. 4b) are complex conjugate due to the coupling of the capacitor voltage. Therefore, no matter the bandwidth of the system is, the closed loop system will always have low damping. For the chosen bandwidth of *1* kHz the regulator gain is approximately $k_{pI} = 5.61$.

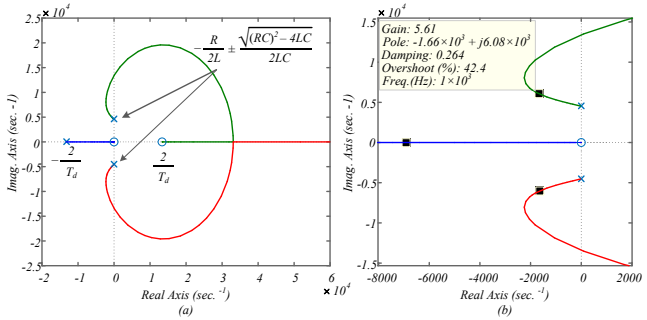

Fig. 4. Root locus for the inner current loop with P regulator and without voltage decoupling: x – open loop poles; ■ closed loop poles for $k_{pI} = 5.61$; o – zeros – (a) complete; (b) zoom

The frequency response (FR) for the inner loop with proportional regulator is shown in Fig. 5. It is difficult to determine the bandwidth of the system because the low frequency behaviour is changing as a function of the frequency, and it is not possible to have a specific value for the gain at low frequencies. However, at short circuit (blue line) the system behaves as an RL load. At this condition, it can be seen that the system bandwidth is approximately 1 kHz, as designed.

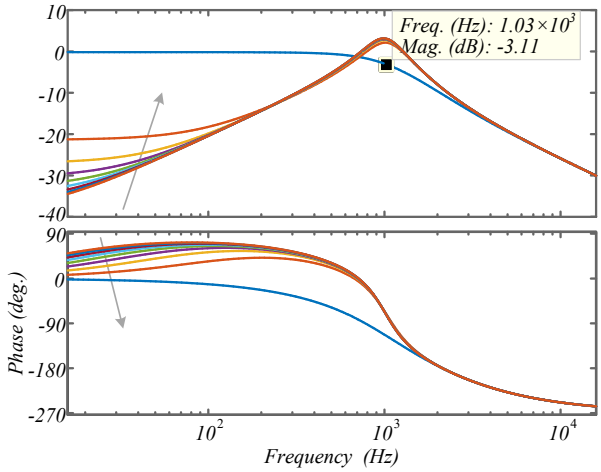

Fig. 5. Closed loop FR for the inner current loop: P regulator without voltage decoupling: effect of the load – arrows indicate increasing in load (from low load to short circuit)

The main conclusions of this analysis are: *i*) The capacitor coupling produces a load dependent dynamics; *ii*) Even with a proportional regulator the resulted closed loop system has a very low damping exactly because of the capacitor voltage coupling; *iii*) The P regulator is unable to achieve zero steady-state error at 50 Hz.

To improve the performance of the inner current loop it is possible to modify the regulator topology and decouple the capacitor voltage cross-coupling. The current regulators analyzed in this work are: *i*) ideal PR; *ii*) non-ideal PR, and *iii*) complex vector PR. The transfer functions of each regulator are presented in TABLE II. , where $\omega_o = 2\pi 50$ rad/s is the resonant frequency, k_{pI} and k_{iI} the proportional and integral gains of the regulators, and h is the harmonic order to be controlled.

The design of the coefficients for the fundamental frequency of a PR controller can be made starting from the design of a PI regulator employed in the *dq*-rotating reference frame. The PR regulators are just implementations of two of these controllers in the stationary reference frame. The current regulator was tuned by selecting a controller zero approximately equal to the break frequency of the *RL* load, i.e., $k_{iI}/k_{pI} \cong R/L$. The regulator gain was selected to achieve the desired bandwidth (f_{bw}). These will be considered the nominal values in this work. For the bandwidth of 1 kHz these parameters are presented in TABLE III.

TABLE II. INNER VOLTAGE/CURRENT LOOP CONTROLLERS

Non-ideal PR	Ideal PR	Complex vector PR
$k_{pI} + \frac{2\omega_c k_{iI} s}{s^2 + 2\omega_c s + (h\omega_o)^2}$	$k_{pI} + \frac{k_{iI} s}{s^2 + (h\omega_o)^2}$	$\frac{k_{pI} s^2 + k_{iI} s}{s^2 + (h\omega_o)^2}$

TABLE III. REGULATOR NOMINAL PARAMETERS VALUES

Parameter	Symbol	Value
Proportional gain	k_{pI}	5.61
Integral gain	k_{iI}	311
Damping term	ω_c	5 rad/s

III. FREQUENCY RESPONSE ANALYSIS WITHOUT VOLTAGE DECOUPLING

The frequency response (FR) for each PR regulator was analysed for different values of the integrator gain k_{iI} to see its influence on the performance. The gain k_{iI} was varied from 11 to 511 to see its effect on the closed loop frequency response. The variation range was chosen based on the values around the one that produces ideally zero-pole cancelation ($k_{iI} = 311$). The effect of the load is neglected by considering a very high value of load impedance in the design (no load condition). For each case, the proportional gain was tuned for a 1 kHz bandwidth.

Fig. 6 shows the closed loop FR for the inner current loop using the non-ideal PR as current regulator. It can be observed that:

1) The ability to produce zero steady-state error at the desired resonant frequency (50 Hz) is dependent of the integrator gain (k_{iI}), the smaller its value the bigger will be the error at 50 Hz;
2) Changes in the resonant frequency (reference of the regulator), while the resonant gain ω_o is kept constant at the tuned resonant frequency, can have a significant impact in the steady-state error, especially if the parameter ω_c is small;

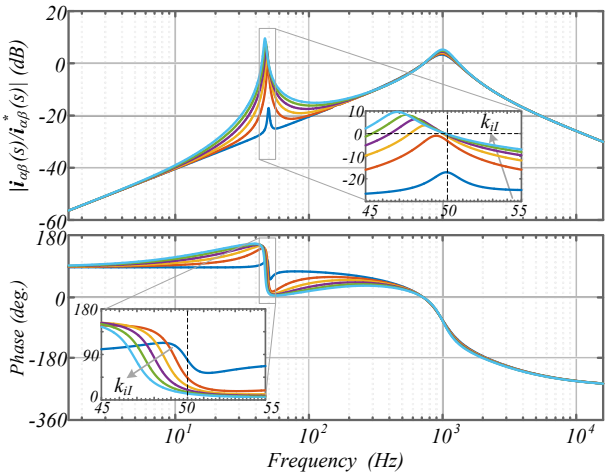

Fig. 6. Closed loop FR of the inner current loop with non-ideal PR regulator and without voltage decoupling: $k_{pI} = 5.6$; $k_{iI} = 11 - 511$ (arrows indicate increasing of k_{iI}).

Fig. 7 shows the closed loop FR for the inner current loop using the ideal PR as regulator. It can be observed that:

1) The regulator is able to produce zero steady-state error at the desired resonant frequency (50 Hz);
2) The system FR is very sensitive to frequency variations (reference of the regulator) around the fundamental frequency. Small changes in frequency (reference of the regulator), while the resonant gain ω_o is kept constant at the tuned resonant frequency, can result in very high steady-state error;
3) The smaller the integrator gain (k_{iI}) the bigger the sensitivity to frequency variation around the resonant frequency (50 Hz) will be.

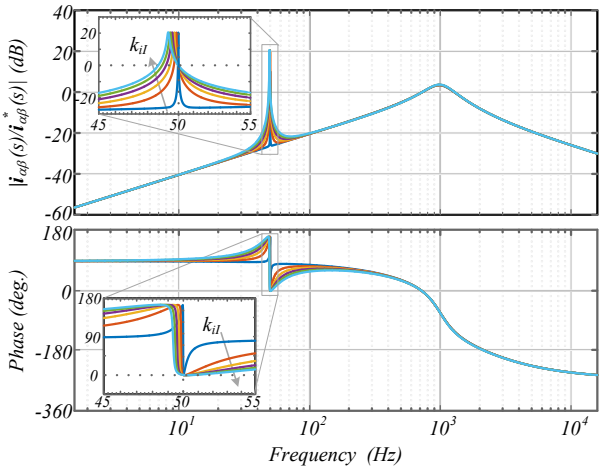

Fig. 7. Closed loop FR of the inner current loop with ideal PR regulator and without voltage decoupling: $k_{pI} = 5.61$; $k_{iI} = 11 - 511$ (arrows indicate increasing of k_{iI}).

When the complex vector PR is used as the current regulator the system is unstable for any value of k_{pI} *or* k_{iI}. As an example, the root locus of the inner current loop for $k_{iI}/k_{pI} = R/L$ is shown in Fig. 8. The root locus is shown just for the dominant poles. As can be seen, the poles are on the right half plane. Therefore, this regulator cannot be used for the case where no decoupling is performed.

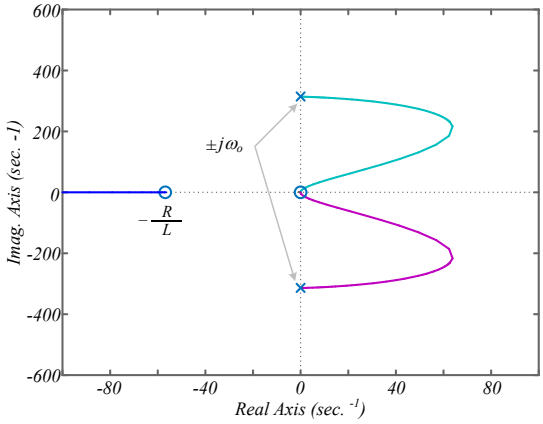

Fig. 8. Root locus of the inner current loop with complex vector PR regulator without voltage decoupling: x – open loop poles; o – zeros; $k_{iI}/k_{pI} = R/L$

The reason why the system (Fig. 3) is unstable is due to the capacitor voltage cross-coupling. Therefore, if a voltage decoupling is performed the complex vector PR can also be used in this system.

IV. Frequency Response Analysis With Voltage Decoupling

If the cross-coupling decoupling is performed ideally by the correct design of the decoupling transfer function $G_{dec}(s)$, the equivalent block diagram of the system is shown in Fig. 9. As result, the load does not affect the current loop anymore. The open loop poles are real, resulting in a closed loop system with bigger damping than for the case without decoupling.

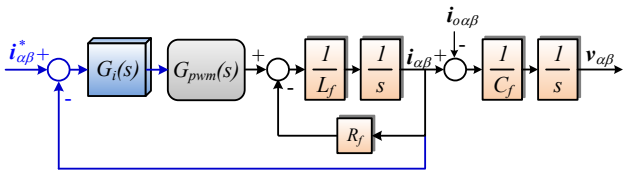

Fig. 9. Simplified block diagram when perfect decoupling is performed.

By using the same bandwidth of 1 kHz, the closed loop FR as a function of k_{iI} is shown in Fig. 10 for the case when the non-ideal PR is used. From this figure, it can be observed that:

1) The controller is almost able to produce zero steady state error at the desired resonant frequency (50 Hz);
2) The smaller the integrator gain (k_{iI}) the bigger will be the error at 50 Hz. However, the error is very small and is fundamentally in the phase, much smaller than the case without voltage decoupling;
3) The system FR has low sensitivity to frequency variations around the resonant frequency. However, the smaller the integrator gain (k_{iI}) the bigger will be the sensitivity around 50 Hz;
4) The corrective effect of the non-ideal PR regulator around the resonant frequency is just 2%;
5) The effect of voltage cross-coupling decoupling is more important than the use of the resonator.

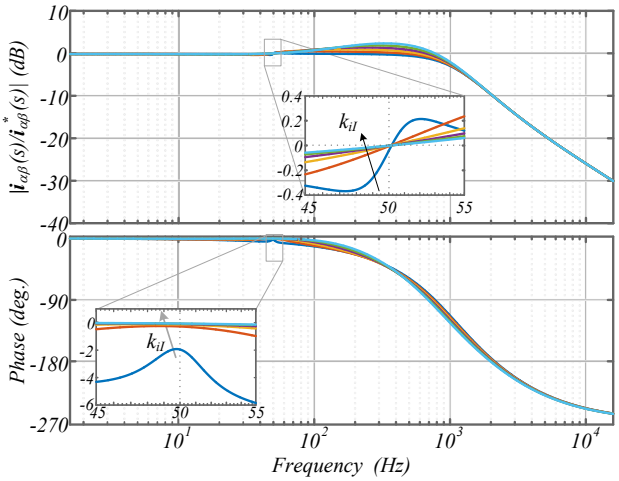

Fig. 10. Closed loop FR of the inner current loop with non-ideal PR regulator, and with voltage decoupling: $k_{pI} = 5.61$; $k_{iI} = 11 - 511$ (arrows indicate increasing of k_{iI}).

Fig. 11 shows the closed loop FR of the inner current loop when the ideal PR regulator is used with output voltage cross-coupling decoupling. The same conclusions as for the case of ideal PR regulator without voltage decoupling can be drawn, except that in this case the variations around the resonant frequency are much smaller. Again, the effect of voltage decoupling is significant.

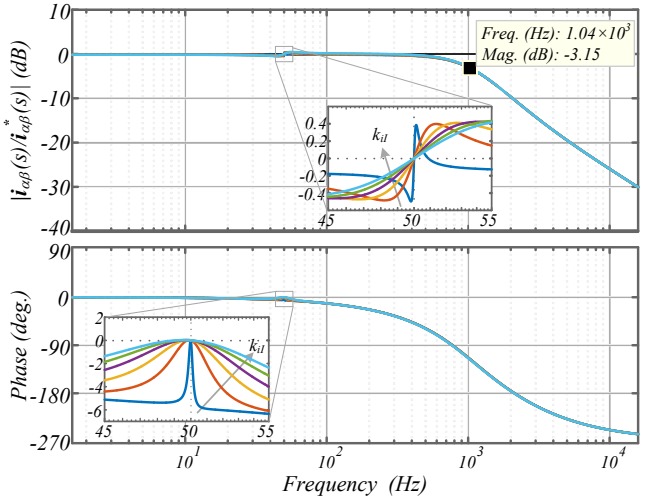

Fig. 11. Closed loop FR of of the inner current loop with ideal PR regulator, and with voltage decoupling: $k_{pI} = 5.61$; $k_{iI} = 11 - 511$ (arrows indicate increasing of k_{iI}).

Fig. 12 shows the closed loop FR of complex vector PR controller with output voltage cross-coupling decoupling. It can be observed that:

1) The controller is able to produce zero steady-state error at the desired resonant frequency (50 Hz);
2) The system FR has low sensitivity to frequency variations around the resonant frequency. Indeed, this sensitivity is smaller than for the cases of ideal and non-ideal PR controllers;
3) The system FR has low sensitivity to the integrator gain (k_{iI}) variations;

Comparing this controller with the others analysed in this paper it is clear that it is the one that presents the lowest sensitivity to frequency variations around the fundamental frequency. Therefore, it is the most indicated for use in applications where the resonant frequency changes as in droop controlled microgrids.

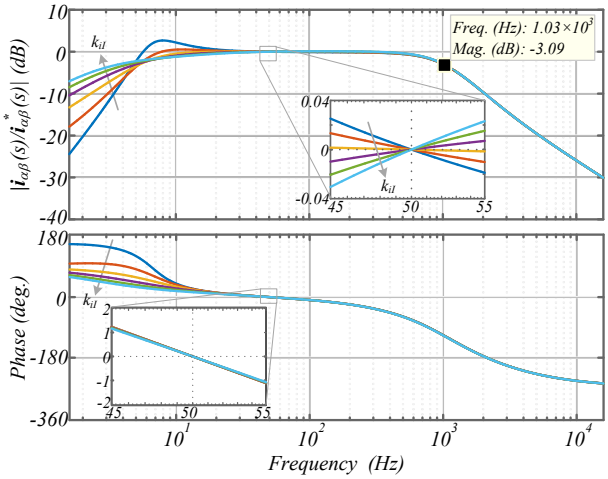

Fig. 12. Closed loop FR of of the inner current loop with complex vector PR regulator, and with voltage decoupling: $k_{pI} = 5.61$; $k_{iI} = 11 - 511$ (arrows indicate increasing of k_{iI}).

V. Experimental Results

The power system of Fig. 1 was tested in the laboratory to check the analysis presented in the previous sections. For this purpose, a 2.2 kW power converter, driven by dSpace DS1006 platform, was used. Therefore, the regulators compared in this work were implemented in discrete time domain.

One important aspect that was not analyzed in previous sections but is relevant when dealing with discrete time systems is the discretization method used for the PR regulators. As an example, one of the possibilities to implement the ideal PR regulator is by using two integrators, as shown in Fig. 13(a) in the continuous time domain and in Fig. 13(b) in the discrete time domain using forward and backward Euler as discretization methods. The main advantage of this structure is its simplicity when frequency variations occur: it is not necessary to calculate online the regulator gains to do frequency adaptation. Another possibility is to use any other discretization method for the transfer function of the regulators (see TABLE II.).

Fig. 14 shows the steady-state currents and errors for ideal PR regulator without and with voltage decoupling for a 5th harmonic reference (250 Hz). The regulator was implemented using two integrators with forward and backward Euler as discretization methods. It can be observed that the regulator does not produce zero steady-state error. Furthermore, the error is bigger when the capacitor voltage is not decoupled (See Fig. 14(a)). On the other hand, Fig. 15 shows the results at the same conditions but with the transfer function of the regulator discretized using impulse invariant method. It is clear the zero steady-state error achieved. This mean that the discretization method is very important when using resonant regulators at high frequencies as is the case when it is desired to perform harmonic compensation.

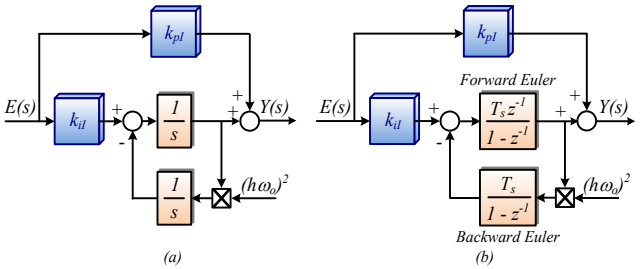

Fig. 13. Block diagram of ideal PR implemented using two integrators: (a) in the continuous time domain; (b) in the discrete time domain using forward and backward Euler as discretization methods

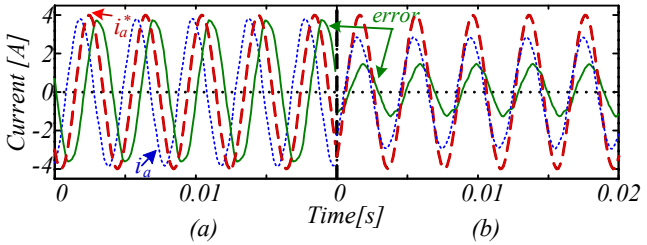

Fig. 14. Steady-state currents and error for ideal PR when implemented with two integrators using forward and backward Euler - 5th harmonic reference tracking: (a) without voltage decoupling; (b) with voltage decoupling

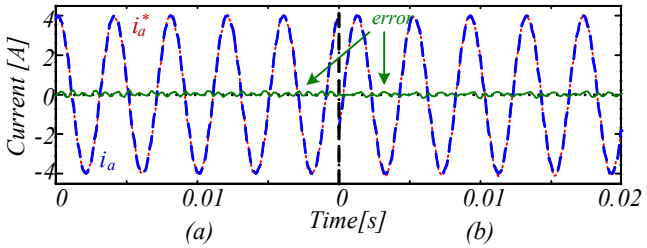

Fig. 15. Steady-state currents and error for ideal PR when the transfer function of the regulator is discretized using impulse invariant method - 5th harmonic reference tracking: (a) without voltage decoupling; (b) with voltage decoupling

As expected from the FR analysis all the three controllers produce approximately zero steady-state error when designed to have exactly the same resonant frequency as the one of the reference current, and with sufficient high k_{iI} as the one presented in Table III. It must be remarked that they should be discretized using the correct method.

To analyze the sensitivity of the PR regulators to frequency variations the reference current frequency was changed to 49

Hz, while the resonant frequency of the regulators was kept constant in 50 Hz. Fig. 16 and Fig. 17 show the steady-state currents and errors for the ideal and non-ideal PR regulators without and with voltage decoupling. It is clear that the effect of voltage decoupling has a significant impact on the performance of the closed loop system, reducing significantly the error. Furthermore, the sensitivity of the ideal PR to frequency variations is bigger than the sensitivity of the non-ideal PR. For this last regulator the zero steady-state error with voltage decoupling depends on the value of k_{iI}. Fig. 18 shows an experimental result for the non-ideal PR with $k_{iI} = 11$. For small values of this gain, the regulator does not provide zero steady-state error, even with voltage decoupling.

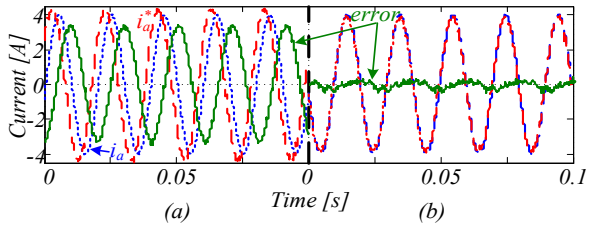

Fig. 16. Steady-state currents and error for ideal PR: (a) without voltage decoupling; (b) with voltage decoupling -$f_{ref} = 49\ Hz$, $k_{iI} = 311$

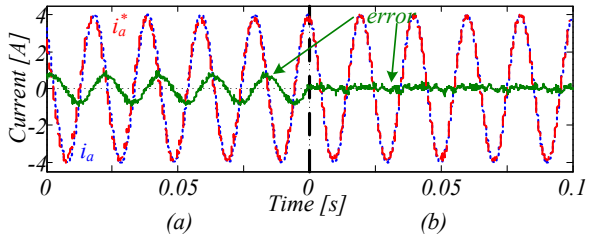

Fig. 17. Steady-state currents and error for non-ideal PR: (a) without voltage decoupling; (b) with voltage decoupling -$f_{ref} = 49\ Hz$, $k_{iI} = 311$

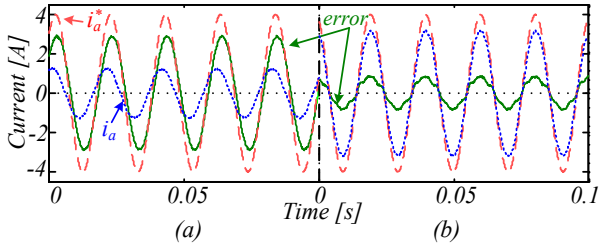

Fig. 18. Steady-state currents and error for non-ideal PR: (a) without voltage decoupling; (b) with voltage decoupling -$f_{ref} = 49\ Hz$, $k_{iI} = 11$

Fig. 19 shows the results for the complex vector PR. As expected from FR analysis, this controller produces zero steady-state error even for small values of k_{iI}, and frequency variations.

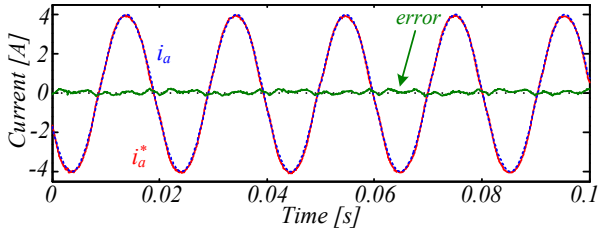

Fig. 19. Steady-state currents and error for compex vector PR with voltage decoupling - $f_{ref} = 49\ Hz$, $k_{iI} = 11$

VI. Conclusions

In this paper, an analysis and design of the inner current loop for power converters based on PR regulators has been carried out. The benefits of applying capacitor voltage decoupling are motivated by the lower steady-state error. Complex vector PR regulator, which is stable only if voltage decoupling is performed, shows the lowest sensitivity to integral gain and frequency deviation, thus can be preferred in microgrid applications.

Acknowledgment

The authors would like to thanks the motivation and support provided by CNPq/Brazil, CEMAR, and University of Aalborg.

References

[1] D. G. Holmes, T. A. Lipo, B. P. McGrath, and W. Y. Kong, "Optimized Design of Stationary Frame Three Phase AC Current Regulators," *Power Electronics, IEEE Transactions on,* vol. 24, pp. 2417-2426, 2009.

[2] C. Lascu, L. Asiminoaei, I. Boldea, and F. Blaabjerg, "High Performance Current Controller for Selective Harmonic Compensation in Active Power Filters," *Power Electronics, IEEE Transactions on,* vol. 22, pp. 1826-1835, 2007.

[3] J. C. Vasquez, J. M. Guerrero, M. Savaghebi, J. Eloy-Garcia, and R. Teodorescu, "Modeling, Analysis, and Design of Stationary-Reference-Frame Droop-Controlled Parallel Three-Phase Voltage Source Inverters," *Industrial Electronics, IEEE Transactions on,* vol. 60, pp. 1271-1280, 2013.

[4] T. M. Rowan and R. J. Kerkman, "A New Synchronous Current Regulator and an Analysis of Current-Regulated PWM Inverters," *Industry Applications, IEEE Transactions on,* vol. IA-22, pp. 678-690, 1986.

[5] D. N. Zmood and D. G. Holmes, "Stationary frame current regulation of PWM inverters with zero steady-state error," *Power Electronics, IEEE Transactions on,* vol. 18, pp. 814-822, 2003.

[6] K. Hongrae, M. W. Degner, J. M. Guerrero, F. Briz, and R. D. Lorenz, "Discrete-Time Current Regulator Design for AC Machine Drives," *Industry Applications, IEEE Transactions on,* vol. 46, pp. 1425-1435, 2010.

[7] J. Holtz, Q. Juntao, J. Pontt, J. Rodriguez, P. Newman, and H. Miranda, "Design of fast and robust current regulators for high-power drives based on complex state variables," *Industry Applications, IEEE Transactions on,* vol. 40, pp. 1388-1397, 2004.

[8] A. G. Yepes, F. D. Freijedo, J. Doval-Gandoy, Lo, x, O. pez, *et al.*, "Effects of Discretization Methods on the Performance of Resonant Controllers," *Power Electronics, IEEE Transactions on,* vol. 25, pp. 1692-1712, 2010.

[9] A. G. Yepes, F. D. Freijedo, O. Lopez, and J. Doval-Gandoy, "Analysis and Design of Resonant Current Controllers for Voltage-Source Converters by Means of Nyquist Diagrams and Sensitivity Function," *Industrial Electronics, IEEE Transactions on,* vol. 58, pp. 5231-5250, 2011.

[10] L. A. S. Ribeiro, M. W. Degner, F. Briz, and R. D. Lorenz, "Comparison of carrier signal voltage and current injection for the estimation of flux angle or rotor position," in *Industry Applications Conference, 1998. Thirty-Third IAS Annual Meeting. The 1998 IEEE*, 1998, pp. 452-459 vol.1.

[11] F. Briz, M. W. Degner, and R. D. Lorenz, "Analysis and design of current regulators using complex vectors," *Industry Applications, IEEE Transactions on,* vol. 36, pp. 817-825, 2000.